

Two-Mode EHD Stimulation of a Continuous Jet: Generation of Drops and Satellites

B. Barbet^{1,2,†}, P. Atten² and A. Soucemarianadin^{1,3†}*

¹ *TOXOT Science & Applications (IMAJE Groupe),
BP 110, 26501 Bourg les Valence (France)*

² *L.E.M.D - CNRS & Univ. J. Fourier, BP 166, 38042 Grenoble Cedex 9 (France)*

³ *Laboratoire de Rhéologie - CNRS & Univ. J. Fourier, BP 53X,
38041 Grenoble Cedex (France)*

Abstract

This study reports the results of work carried out to investigate the high-frequency periodical break-up process of a liquid jet using an electrohydrodynamic (EHD) multimode jet stimulation device. The aims of this study were to optimize the different parameters and to generate droplets of conducting fluid in a controlled fashion. In particular, the experiments were performed for wavenumbers $k \leq 0.5$ with the second harmonic purposely introduced in the excitation signals. A dimensional analysis applied to the problem provided the main dimensionless parameters whose influence on jet break-up mechanisms were examined. We found different regimes of break-up depending on both the electrostatic pressure ratio and the phase shift between the fundamental and the second harmonic. In addition, various patterns of drop production and boundaries between regions of parameter space with different drop break-up behaviors were clearly identified using image processing techniques. Other features of jet break-up such as satellite droplet diameters and lifetimes were also considered in detail. Finally, our focus was to find the most suitable conditions for jet printer operation.

Introduction

Continuous ink-jet technology requires formation of drops from a jet at a well-defined frequency. Piezoelectric stimulation has been used to produce velocity disturbances that grow through surface tension forces until the jet breaks up into uniform drops.¹ Although this type of stimulation may allow formation of a stream of drops devoid of satellites, a noticeable disadvantage is acoustic crosstalk when operated in multijet devices.² But use of electrohydrodynamic (EHD) exciters,^{3,4} which are easier to design because the excitation is downstream from the nozzle, could be preferable in multijet printers. A well-known limitation of this type of excitation is the occurrence of secondary droplets or so-called satellites that are deleterious for appropriate printing because they lead to drop placement errors in the final image. It has been shown both in the case of acoustic and EHD exciters^{5,6} that the for-

mation of satellite droplets is controlled by interactions between the harmonics of the fundamental excitation. The harmonics could either arise because of nonlinear fluid mechanical effects related to the excitation mode; nozzle effects;⁷ or be introduced purposely into the jet by the EHD exciters,⁶ for example.

In this study, following Rezanka and Crowley,⁶ we present results on the EHD stimulation of a continuous jet using two modes of frequency f and $2f$. More particularly, we perform experiments with various electrode configurations at different wavenumbers using well-characterized fluids. We first perform a dimensional analysis of the problem followed by a detailed presentation of our various drop generation set-ups, one of which has been used previously both for multielectrode continuous EHD stimulation⁴ and for pulsed EHD excitation.⁸ We then provide a discussion of the different regimes of break-up obtained with a scaled-up generator which is easy to use. In particular, we study the influence of the ratio of the disturbance amplitudes and the phase shift between the two modes. We also present selected results for operating conditions that allow or suppress the formation of satellites. Experiments are performed with different jet diameters for those regions of particular interest for ink-jet printing, which give similar results when appropriate dimensionless numbers are taken into account. We summarize the main findings in the conclusions.

Problem Description and Dimensional Analysis

The electrohydrodynamic stimulation of a cylindrical jet submitted to a periodical electrical voltage applied either on one or several electrodes is shown in Fig. 1. The electrostatic pressure applied onto the surface of the jet is then also periodical with the electrodes exerting an axisymmetric radial perturbation onto the jet. The assumptions made are that the flow is substantially one-dimensional and viscous. If, moreover, we assume the velocity and pressure are dependent only on axial coordinate x and time t , then the hydrodynamic equation of momentum reads:

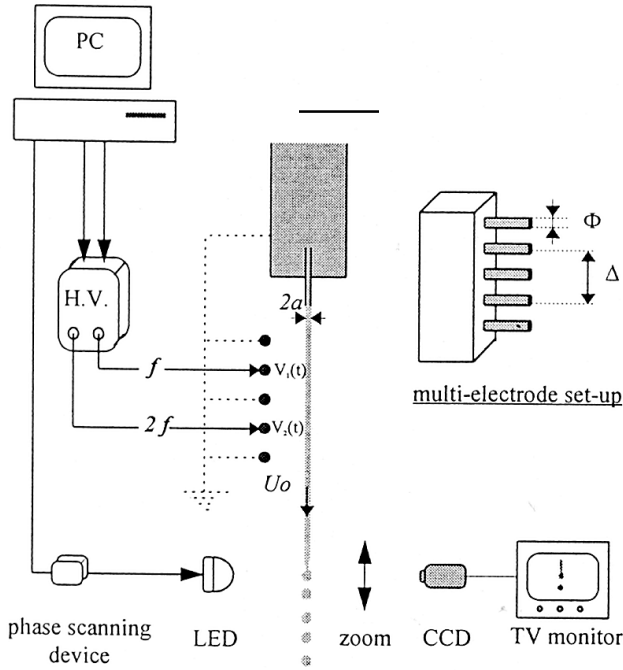


Figure 1. Schematic representation of the jet stimulation device.

$$\frac{\partial u}{\partial t} + u \frac{\partial u}{\partial x} = -\frac{1}{\rho} \frac{\partial}{\partial x} (P_s + P_e) + \nu \frac{\partial^2 u}{\partial x^2} \quad (1)$$

where u is the jet velocity, ρ the fluid density, P_s the capillary pressure, P_e the electrostatic pressure induced by the periodic voltage, and ν the fluid kinematic viscosity.

Table I lists the dimensional parameters introduced in the above equation to which we must add the stimulating frequency to account for the pulsating nature of the flow. According to Buckingham's π theorem,⁹ the number of dimensionless groups governing the flow is then four [(7 parameters) – (3 dimensions)]. The groupings are formed according to the law of dimensional homogeneity and lead to the following dimensionless numbers (Weber, Reynolds, Strouhal, and electrical Euler), with their values listed in Table II.

$$We = \frac{\rho U_0^2 a}{\sigma}, \quad Re = \frac{\rho U_0 a}{\mu}, \quad Str = \frac{fa}{U_0}, \quad Eu_e = \frac{P_e}{\rho U_0^2} \quad (2)$$

The experiments reported here were performed both with a scaled-up drop generator, henceforth, called model, and an industrial ink-jet printer, which is the prototype. The model serves to characterize the drop formation behavior while the prototype validates the results useful for printing applications. In this respect, the dimensionless parameters should be maintained equal between the two sets of experiments (model and prototype).

Experimental

A typical example of the devices used in this work is shown in Fig. 1. The jet ($2a$ in diameter) emerges either from a short

TABLE I. Experimental Set-Ups: Dimensional Parameters

		Model	Prototype
Jet radius [μm]	a	220	35
Jet velocity [m/s]	U_0	5	11.5
Viscosity [mPa.s]	μ	17	6.35
Surface tension [mN/m]	σ	57	45
Density [Kg/m^3]	ρ	1165	1130
Frequency [Hz]	f	723	10,600
Electrostatic pressure [Pa]	Pe	21	70

TABLE II. Typical Dimensionless Numbers of the Experimental Set-Ups

		Model & Prototype
Reynolds	Re	76
Weber	We	116
Strouhal	Str	0.064
Electrical Euler	Eu_e	0.0006

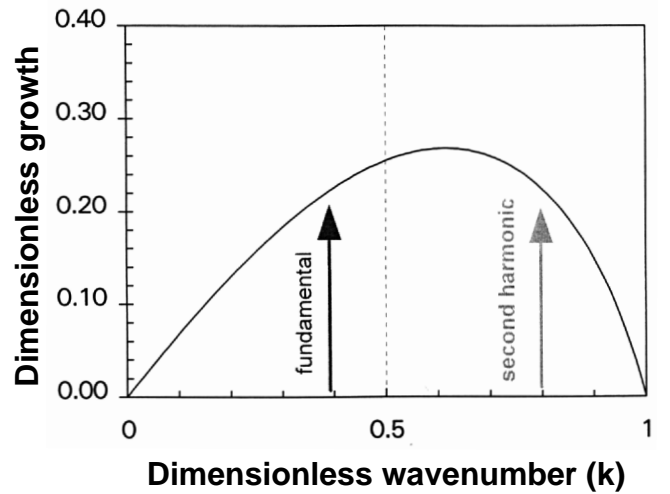


Figure 2. Conditions of amplification for the stimulating frequencies.

($1/2a = 1$) or a long ($1/2a = 20$) nozzle. The jet velocity (U_0) is carefully controlled by means of a pressure-regulated tank feeding the fluid. The stimulation electrodes located downstream from the nozzle consist of a set of five steel rods. Electrodes 1, 3, and 5 are grounded (Fig. 1). The signal applied to Electrode 2 is at frequency f while that of Electrode 4 is at frequency $2f$. We chose to work at a dimensionless wavenumber $k = (2\pi a/\lambda) < 0.5$ (λ is the wavelength) to amplify the second harmonic. Moreover, the two frequencies are such that the dimensionless growth rate values are the same for both wavenumbers as shown in Fig. 2.

In contrast to Rezanka and Crowley⁶ we are able to stimulate the jet with simple sinusoids. Moreover, with our electrode configuration, we are not limited in the order of the harmonic that can be introduced into the jet. The two different waveforms of the driving voltages are simultaneously synthesized using custom software. The digital signals are first converted to analog and used to drive two high-voltage amplifiers. The outputs from the amplifiers have the following form:

$$V_1(t) = V_1 \cos(\pi f t) \quad \text{and} \quad \frac{1}{2}(t) = V_2 \cos\left(2\pi f t + \frac{\phi}{2}\right) \quad (3)$$

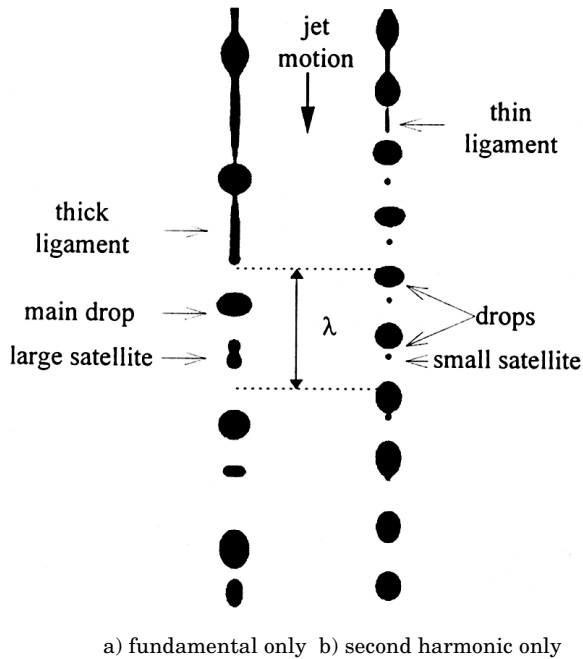


Figure 3. Jet break-up patterns: (a) fundamental only $P_2/P_1 = 0$, second harmonic only $P_2/P_1 = 0$.

The electrostatic pressure $P_i(t)$ (attractive force on the surface of the jet) is proportional to $V_i^2(t)$. The disturbance applied onto the jet is the fundamental for the first electrode and is the second harmonic for the electrode located downstream. This introduces a spatial phase shift depending on both the jet velocity U_0 and the distance Δ between the two stimulating electrodes. Finally, the stimulating electrostatic pressure reads:

$$P(t) = P_1 \cos(2\pi ft) + P_2 \cos(2 * 2\pi ft + \phi) \quad (4)$$

where ϕ is the real phase shift experienced by the jet surface: $\phi = \phi - 2\pi f \Delta / U_0$.

The ink-jet break-up is studied using a visualization technique described elsewhere.⁴ The microcomputer used to generate the electrode signals also triggers a strobe light (LED) that allows the observation of the magnified jet profile on a video display. The mean velocity U_0 of the jet is determined from the relationship $U_0 = \lambda f$. To observe closely the break-up of the jet and the formation and lifetime of the satellites, we introduce a variable phase shift between the electrode triggering signals and those of the LED. This allows us to strobe the jet at different relative times, i.e., at different axial locations. The life lengths (distances covered before merging) of satellites are read on a digital display connected to the translation stage holding the nozzle, whereas their diameters are found from a shadow method using a slit of known dimensions.⁷

The fluids used are dyed glycerine-water mixtures. The presence of the dye allows us to obtain a conductivity σ sufficient for EHD stimulation of the jets. Table I lists the main parameters used in the experiments presented in the following. Note that the principal dimensionless numbers derived above are maintained the same for both model and prototype.

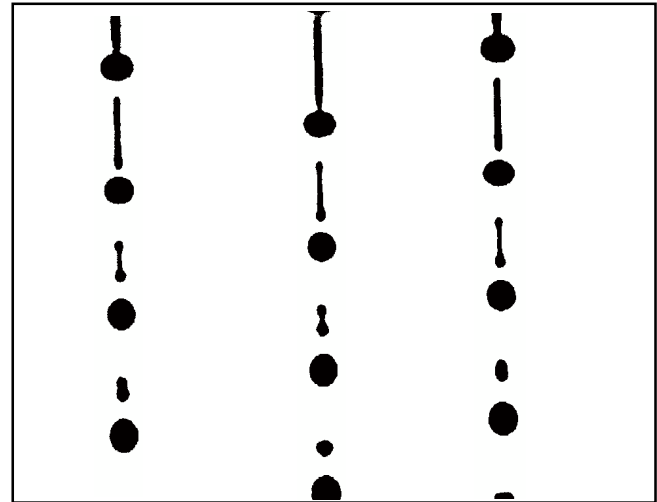


Figure 4. Fore- and aft-side break-up followed by a ligament collapse leading to the formation of a large satellite.

Two-Mode EHD Stimulation of a Continuous Jet

Different Regimes of Break-Up. As noticed by Rezanka and Crowley⁶, different regimes exist depending on both the ratio of the electrostatic pressure P_1/P_2 and the phase shift ϕ . For very small values of P_2/P_1 ($\ll 1$), the break-up is determined by the fundamental stimulating mode and there are two droplets per wavelength λ : one main drop and one large satellite [see Fig. 3(a) and bottom left corner of Fig. 6]. When the second mode is predominant ($P_2/P_1 \gg 1$), there are four droplets per wavelength λ , corresponding to the mode $2f$: two drops and two small satellites [(see Fig. 3(b) and top right corner of Fig. 6)]. For some intermediate values of P_2/P_1 , we may expect three droplets. The region of particular interest in ink-jet printing is where only one drop is generated. It is therefore important to delineate the different modes of drop production in the map P_2/P_1 versus ϕ .

Such a map is given in Fig. 6 for the wavenumber $k = 0.400$. It shows the various regions in the stimulation parameter plane leading to one, two, three, or four droplets. Inserted in this figure, are photographs showing three wavelengths of the jet in the break-up area to illustrate typical figures of jet deformation and break-up.

For $\phi = 300^\circ$. Increasing P_2/P_1 from zero results first in a large satellite that slows down until there is no separation from the main drop (fore-side break-up only which leads to a no-satellite zone for $0.17 < P_2/P_1 < 0.29$ delineated by the bold line). This is the appropriate zone for ink-jet printing. For $P_2/P_1 > 0.29$ the ligament (see Fig. 3) gives rise to a small satellite that coalesces with the following drop (slow satellite behavior). At still higher values of the pressure ratio, the

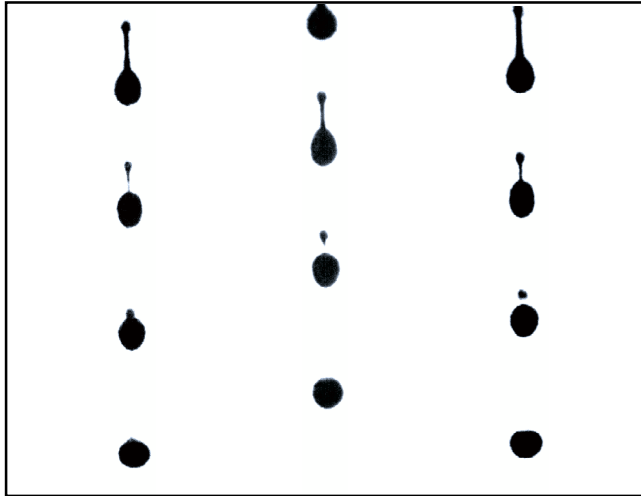


Figure 5. Fore- and aft-side break-up with draining of fluid in the drop leading to the formation of a small satellite.

deformation of the main drop becomes more and more marked until it splits into two drops of similar size ($P_2/P_1 > 4.9$). Finally, for $P_2/P_1 > 5.7$, a microsatellite (much smaller in size than the “small satellite” of Fig. 3) appears in between the two drops (Fig. 6). Note that this succession of regimes remains qualitatively similar for ϕ varying from 260° to 380° .

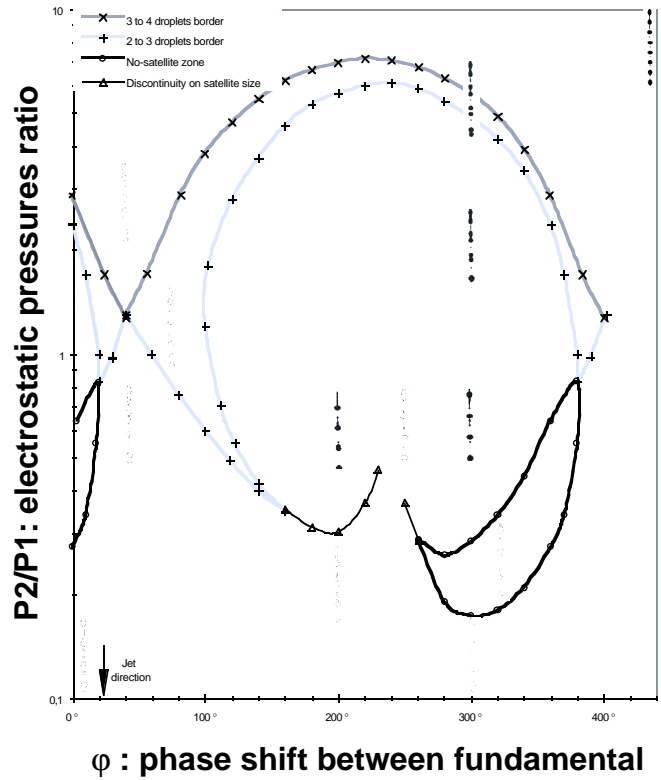


Figure 6. Break-up diagram at wavenumber $k = 0.400$ (jet diameter = $220 \mu\text{m}$).

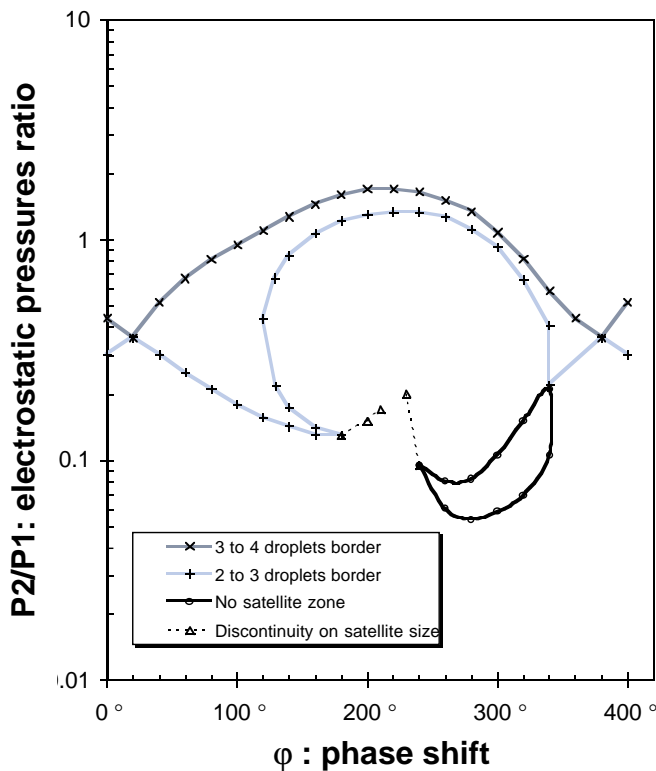


Figure 7. Break-up diagram at wavenumber $k = 0.350$ (jet diameter = $220 \mu\text{m}$).

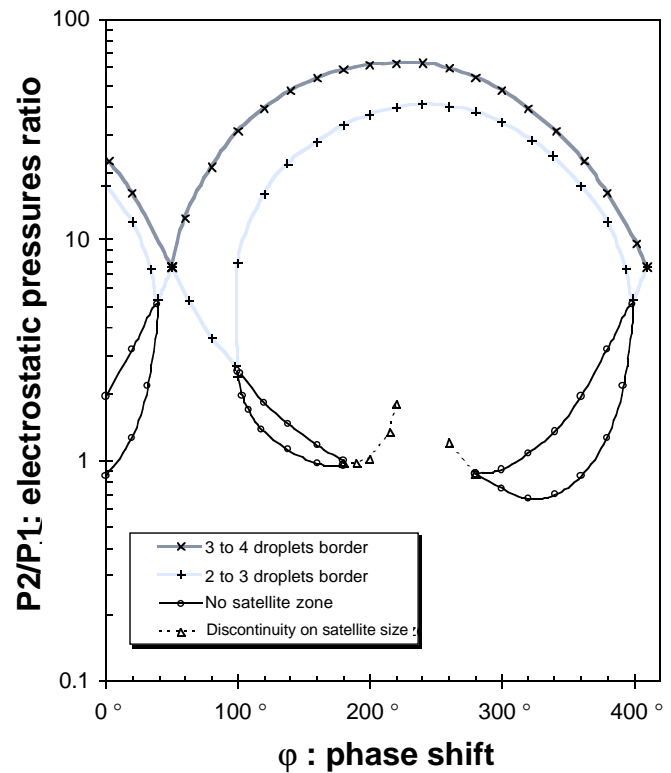


Figure 8. Break-up diagram at wavenumber $k = 0.437$ (jet diameter = $220 \mu\text{m}$).

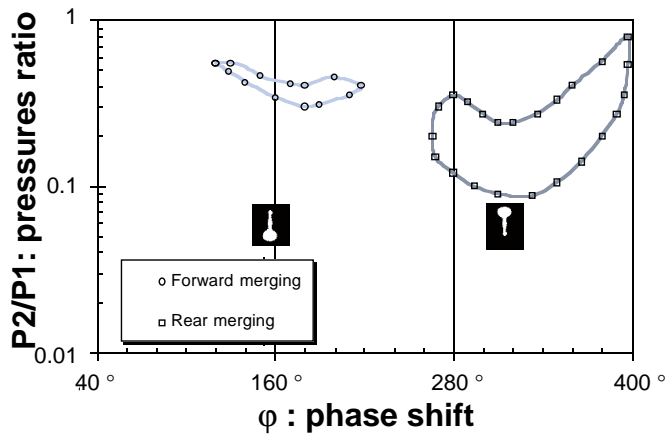


Figure 9. Asymmetrical no-satellite areas corresponding to a low jet velocity.

For $\phi = 180^\circ$. In increasing the electrostatic pressure ratio, the large satellite becomes fast coalescing with the main preceding drop (this is called forward merging). In Fig. 4 we notice that drop break-up occurs simultaneously at both ends. Thanks to representation at different relative times obtained using the phase-scanning device (Fig. 1), ligament contraction can be followed to the formation of a single large satellite. At $P_2/P_1 = 0.3$ it is noticeable (Fig. 5) that the satellite tends to merge into the main drop but simultaneously a part of the ligament is stretched and breaks up leading to a small satellite. In this case, for k equal to 0.400, we did not encounter a no-satellite zone as reported in Rezanka and Crowley.⁶ Various reasons for this difference are discussed later.

For P_2/P_1 increasing above 0.31, the phenomena are similar to those at $\phi = 300^\circ$ except that the small satellite is fast at lower P_2/P_1 one and slow at higher P_2/P_1 . The break-up occurs with the pear-like shape of the main drop facing the nozzle (aft-side break-up followed by a fore-side one leading to a fast satellite). The two dashed lines extending from $\phi = 160^\circ$ to 230° and $\phi = 255^\circ$ to 265° characterize a discontinuous change from the large satellite to the small. At two critical points ($\phi = 230^\circ$ and 255°) this discontinuity ceases. Indeed, for the transition between both behaviors ($\phi = 250^\circ$), the large infinite satellite smoothly becomes small one $P_2/P_1 = 0.6$.

Outside the central loop zone, i.e., for $20^\circ < \phi < 100^\circ$ the phenomena are simpler and a transition occurs from two to three and then four droplets as P_2/P_1 is increased, except at the singular point ($\phi \approx 40^\circ$) where one skips directly from two to four droplets.

Influence of the Wavenumber on Drop Break-Up. As stated in the introduction, it is an essential requirement for technological reasons to obtain drop formation devoid of satellites. In their work, Rezanka and Crowley⁶ noticed two zones of no-satellite operating conditions for wavenumber $k = 0.406$. In nearly similar conditions (wavenumber $k = 0.400$), we obtain the zone between 260° and 380° , but the zone near $\phi = 180^\circ$ is absent (Fig. 6). This different behavior can perhaps be attributed to the effect of scale-up. We hypothesize that the hydrodynamics may not be exactly the same for the detachment and merging

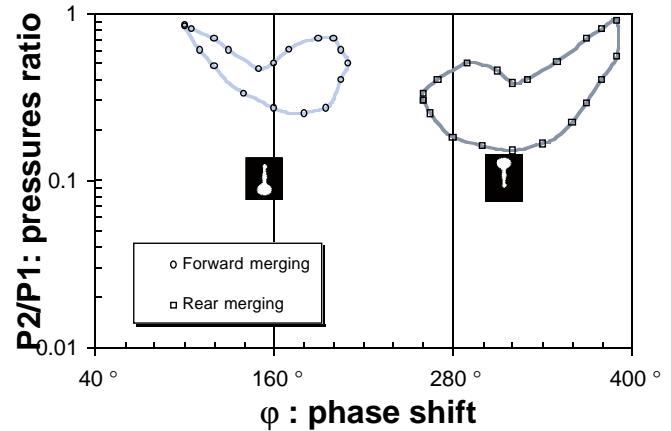


Figure 10. Symmetrical no-satellite areas corresponding to a high jet velocity.

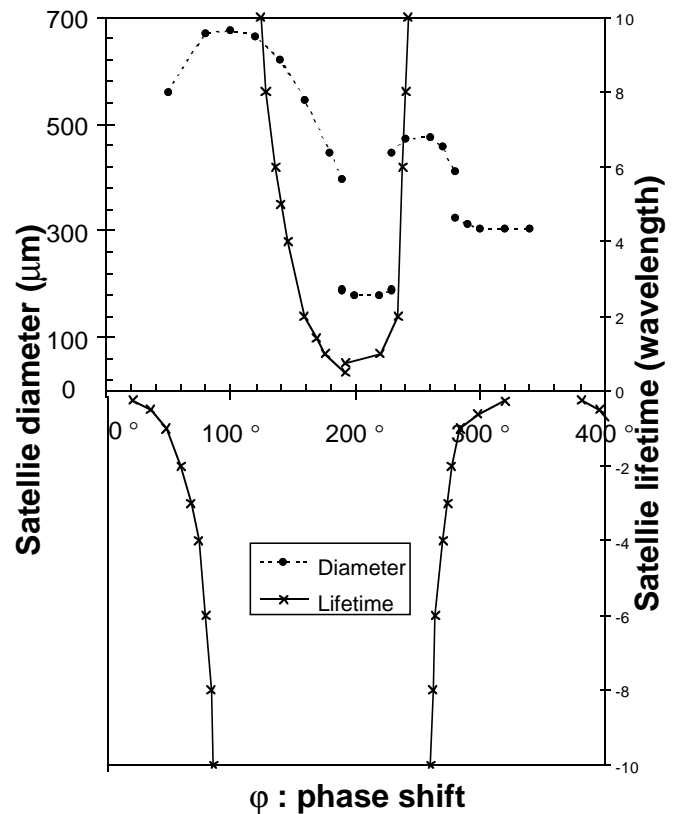


Figure 11. Satellite patterns for $P_2/P_1 = 0.33$ and $k = 0.400$.

of much larger filaments than those usually found in ink-jet printing.^{10,11}

Another possible reason for the difference from Rezanka and Crowley's⁶ results is that our wavenumber is slightly different from theirs. So we performed experiments at two other different wavenumbers [$k = 0.350$ (Fig. 7) and 0.437 (Fig. 8)]. For $k = 0.350$, in comparison with 0.400 , the zone with three droplets is larger, which means that drop and ligament break-up occur almost simultaneously. Indeed, the length of the ligament is such that it is unstable and thus, always ends

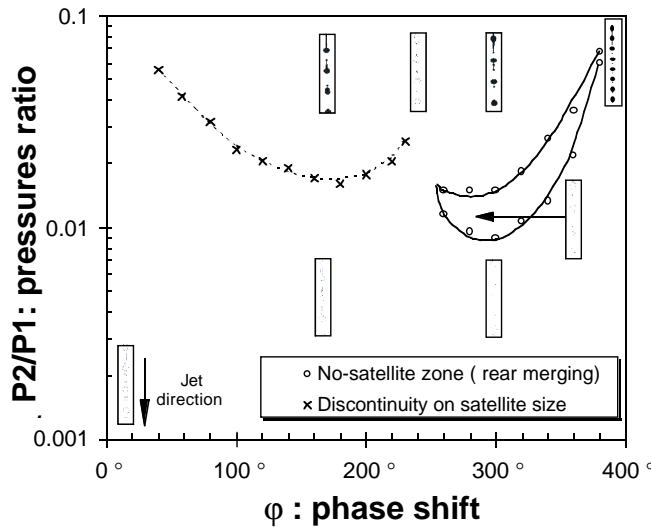


Figure 12. Application to ink jet printing: same diagram as in Fig. 6 but with a jet diameter of 72 μm .

with its break-up. For $k = 0.437$, we succeed in finding a no-satellite zone for the forward merging process (ϕ between 100° and 180°). The discrepancies with the observations of Rezanka and Crowley⁶ lie in the shapes and the abscissae locations of the no-satellite zones. This value of $k = 0.437$ seems optimal in printing applications because the drop size is smaller and the break-up length shorter.

Influence of Jet Velocity on Drop Break-Up. Until now we have not really considered the effect of jet velocity which may be of some importance in drop break-up mechanisms because it distinguishes temporal instability from the spatio-temporal one. So we performed experiments at different jet velocities while maintaining a constant wave-number. By

increasing the jet velocity, we note for the no-satellite zones (Figs. 9 and 10) that the break-up tends to become more symmetrical, i.e., an increase in the area of the aft-side break-up zone ($\phi = 180^\circ$) is balanced by a decrease in the area of the fore-side break-up zone ($\phi = 300^\circ$) and vice versa. We note that comparison with the results of Rezanka and Crowley⁶ become more favorable at higher velocity. This is consistent with the fact that their Reynolds and Weber numbers are higher^{6,12} than those reported in Table II. Therefore, the wavenumber alone is not sufficient to account fully for the drop break-up mechanisms. More experiments are needed to resolve the importance of each of the above dimensionless parameters in drop break-up mechanisms.

Lifetime and Size of Satellite Droplets. We also present in Fig. 11 typical experiments performed at various phase shifts for fixed amplitude ratio $P_2/P_1 = 0.31$ and constant wavenumber $k = 0.400$. For $\phi = 0^\circ$ we encounter the no-satellite zone delineated by the bold line of Fig. 6. For increasing values of ϕ , a very short life satellite is first noted at $\phi = 20^\circ$. The satellite lifetime given in wavelengths (positive lifetime is related to a fast satellite, negative lifetime to a slow one) begins to increase from $\phi = 40^\circ$ to $\phi = 100^\circ$ (infinite satellite and maximal diameter). The satellite lifetime slowly decreases when the phase shift $\phi = 180^\circ$. At this point, as already mentioned there is creation of a small satellite with minimal lifetime. The creation process of the small satellite is first a separation on the aft side followed by some liquid being drained into the main front drop. This explains the sharp decrease in satellite diameter observed for $\phi = 190^\circ$. Diameter discontinuities found for the particular amplitude ratio investigated reflect different break-up mechanisms. The smaller satellite diameters are found for $180^\circ < \phi < 220^\circ$ and $280^\circ < \phi < 320^\circ$ with break-up occurring with mass transfer as stated above. The maxima in satellite diameters are for $\phi = 100^\circ$ and 260° where a double-end pinch-off process without mass transfer takes place.

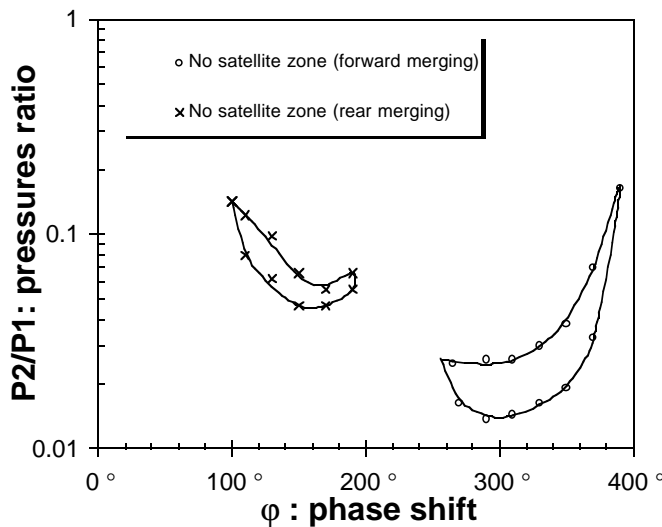


Figure 13. Application to ink jet printing: same diagram as in Fig. 8 but with a jet diameter of 72 μm .

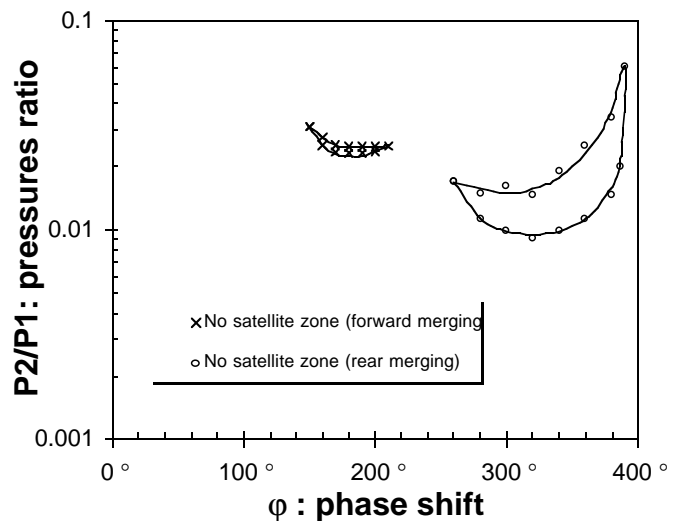


Figure 14. Application to ink-jet printing: same diagram as in Fig. 10 but with a jet diameter of 72 μm .

Application to Ink-Jet Printing

Thus far, we have used the scaled-up model for our experiments. Now, we validate our results on the ink-jet printer prototype emphasizing the no-satellite zones of practical importance in ink-jet printing. The different parameters re listed in Table I. The first experiment (Fig. 12) with the prototype is performed at the same dimensionless numbers as those stated in Fig. 6 for the model. The results are quantitatively similar. We find for the prototype, at the expected location (in terms of phase shift), the fore-side break-up devoid of satellites. As already noticed in Fig. 6, the aft-side break-up no-satellite zone is absent. The very good comparisons between model and prototype lead us to say that the dimensional analysis performed correctly represents the nature of the flows. Above we identified the wavenumber (Figs. 7 and 8) and the jet velocity (Figs. 9 and 10) as the essential parameters to change for eventual modification of the no-satellite zones. Figures 13 and 14 show the results for the prototype when varying the above parameters. In particular, by increasing the wavenumber and jet velocity, we demonstrate that the aft-side break-up no-satellite zone can be considerably expanded. In contrast to Rezanka and Crowley's analysis,⁶ we believe no reasons exist a priori to prefer one region of no-satellite to another because we have shown that by varying wavenumber and jet velocity the latitude of any of these regions can be easily controlled.

Conclusions

An experimental investigation of the break-up of an ink jet submitted to harmonic EHD stimulation led to a variety of drop break-up patterns. We determined the break-up maps for various wavenumbers and jet velocities as a function of both the electrostatic pressure ratio and the phase shift between the fundamental and the second harmonic of the stimulation signal. Several discrepancies appearing with the work of Rezanka and Crowley were noted and explained. Moreover, other features of the jet break-up process such as satellite sizes and lifetimes were considered in detail. The experiments performed with different jet diameters demonstrate the crucial role played by jet velocity in defining the

boundaries of no-satellite zones. This allowed us to propose optimal operating conditions for ink-jet printers in terms of drop break-up.

Acknowledgements. We wish to thank the management of TOXOT Science & Applications for permission to publish this paper and especially A. Dunand for helpful comments. We also thank the Centre National de la Recherche Scientifique (CNRS) for partially funding the study (contract CNRS/IMAJE No. 50.9776). This study has also received partial financial support from the Ministère de la Recherche et de l'Enseignement Supérieur under Grant No. 92 P 0645. B. Barbet's Ph. D. thesis work was performed under CIFRE/ANRT Grant No. 032/94.

References

1. G. L. Fillmore and D. C. Van Lokeren, *IEEE-IAS Conference Proceedings* (October 4–8, 1982).
2. A. Badea, A. Dunand, A. Soucemarianadin, and C. Carrasso, in *IS&T 9th Intl. Congress on Advances in Non-Impact Printing Technologies*, IS&T, Springfield, VA, 1993, pp. 256–259.
3. J. M. Crowley, *IEEE Trans. Ind. Appl.*, **6** 973–976 (1986).
4. A. Spohn, P. Atten, A. Soucemarianadin, and A. Dunand, in *IS&T 9th Intl. Congress on Advances in Non-Impact Printing Technologies*, IS&T, Springfield, VA, 1993, p. 294.
5. K. C. Chaudary and T. Maxworthy, *J. Fluid Mech* **96** (3) 287 (1980).
6. I. Rezanka and J. M. Crowley, *J. Imaging Sci. Technol.* **16** (1) (1990).
7. J. H. Xing, A. Boguslawski, A. Soucemarianadin, P. Atten, and P. Attané, *Exp. Fluids* **20** (4) 302 (1996).
8. C. Bardeau, D. Fressard, P. Atten, and B. Barbet, in *IS&T 10th Intl. Congress on Advances in Non-Impact Printing Technologies* (IS&T, Springfield, VA, 1994) p. 439.
9. G. K. Batchelor, *An Introduction to Fluids Dynamics*, Cambridge University Press, Cambridge, MA, 1981, p. 211.
10. S. A. Curry and H. Portig, *IBM J. Res. Develop.* **10** (1977).
11. P. Vassallo and N. Ashgriz, *Proc. R. Soc. Lond. A* **433**, 269 (1991).
12. J. M. Crowley, *J. Electrostatics* **14**, 121 (1983).